

Engineered two-dimensional Ising interactions in a trapped-ion quantum simulator with hundreds of spins

Joseph W. Britton¹, Brian C. Sawyer¹, Adam C. Keith^{2,3}, C.-C. Joseph Wang², James K. Freericks², Hermann Uys⁴, Michael J. Biercuk⁵ & John J. Bollinger¹

The presence of long-range quantum spin correlations underlies a variety of physical phenomena in condensed-matter systems, potentially including high-temperature superconductivity^{1,2}. However, many properties of exotic, strongly correlated spin systems, such as spin liquids, have proved difficult to study, in part because calculations involving N -body entanglement become intractable for as few as $N \approx 30$ particles³. Feynman predicted that a quantum simulator—a special-purpose ‘analogue’ processor built using quantum bits (qubits)—would be inherently suited to solving such problems^{4,5}. In the context of quantum magnetism, a number of experiments have demonstrated the feasibility of this approach^{6–14}, but simulations allowing controlled, tunable interactions between spins localized on two- or three-dimensional lattices of more than a few tens of qubits have yet to be demonstrated, in part because of the technical challenge of realizing large-scale qubit arrays. Here we demonstrate a variable-range Ising-type spin–spin interaction, $J_{i,j}$ on a naturally occurring, two-dimensional triangular crystal lattice of hundreds of spin-half particles (beryllium ions stored in a Penning trap). This is a computationally relevant scale more than an order of magnitude larger than previous experiments. We show that a spin-dependent optical dipole force can produce an antiferromagnetic interaction $J_{i,j} \propto d_{i,j}^{-a}$, where $0 \leq a \leq 3$ and $d_{i,j}$ is the distance between spin pairs. These power laws correspond physically to infinite-range ($a = 0$), Coulomb-like ($a = 1$), monopole–dipole ($a = 2$) and dipole–dipole ($a = 3$) couplings. Experimentally, we demonstrate excellent agreement with a theory for $0.05 \lesssim a \lesssim 1.4$. This demonstration, coupled with the high spin count, excellent quantum control and low technical complexity of the Penning trap, brings within reach the simulation of otherwise computationally intractable problems in quantum magnetism.

A challenge in condensed-matter physics is the fact that many quantum magnetic interactions cannot currently be modelled in a meaningful way. A canonical example is the spin liquid, an exotic state postulated¹ to arise in a collection of spin-1/2 particles residing on a triangular lattice and coupled to each other by a nearest-neighbour antiferromagnetic Heisenberg interaction. The spin liquid’s ground state is highly degenerate, owing to spin frustration, and is expected to have unusual behaviours including phase transitions at zero temperature driven by quantum fluctuations¹⁵. However, despite recent advances^{16,17} a detailed understanding of large-scale frustration in solids remains elusive^{2,18–20}.

Atomic physicists have recently provided a bottom-up approach to the problem by engineering the relevant spin interactions in quantum simulators^{5,21,22}. The necessary experimental capabilities—laser cooling, deterministic spin localization, precise spin-state quantum control, high-fidelity read-out and engineered spin–spin coupling—were first demonstrated in the context of atomic clocks (see, for example, ref. 23). In the domain of quantum magnetism, this tool set permits

control of parameters commonly viewed as immutable in natural solids, for example lattice spacing and geometry, and spin–spin interaction strength and range.

Initial simulations of quantum Ising and Heisenberg interactions with localized spins were done with neutral atoms in optical lattices^{6,11}, atomic ions in Paul traps^{9,10,13,14} and photons¹². This work involved simulations readily calculable on a classical computer: interactions between $N \approx 10$ qubits localized in one-dimensional (1D) chains. The move to quantum magnetic interactions on two-dimensional (2D) lattices and between larger, computationally relevant numbers of particles is the crucial next step but at present requires more technological development²⁴.

In our Penning trap apparatus, laser-cooled ⁹Be⁺ ions naturally form a stable 2D Coulomb crystal on a triangular lattice with ~ 300 spins (Fig. 1). Each ion is a spin-1/2 system (qubit) over which we exert high-fidelity quantum control²⁵. In this paper, we demonstrate the use of a spin-dependent optical dipole force (ODF) to engineer a continuously tunable Ising-type spin–spin coupling $J_{i,j} \propto d_{i,j}^{-a}$. This capability, in tandem with a modified measurement routine (for example by more sophisticated processing of images such as that in Fig. 1), is a key advance towards useful simulations of quantum magnetism.

A Penning trap confines ions in a static quadrupolar electric potential (Methods) and a strong, homogeneous magnetic field $\mathbf{B} = B_0 \hat{z}$ ($B_0 = 4.46$ T). Axial trapping (along z) is due to the electric field. Ion rotation at frequency ω_r (about z) produces a radial restoring potential due to the velocity-dependent Lorentz force ($q\mathbf{v} \times \mathbf{B}$, where q and \mathbf{v} are respectively the ion’s charge and velocity). Tuning the ratio of the axial to radial confinement allows controlled formation of a planar geometry and, after Doppler laser cooling, the formation of a 2D Coulomb crystal on a triangular lattice²⁶ (Methods). We routinely generate crystals with N ions ($100 \lesssim N \lesssim 350$), where the valence-electron spin state of each ion serves as a qubit²⁵. Following techniques developed in linear (1D) Paul traps²⁷, spins confined in the same trapping potential are coupled through their shared motional degrees of freedom.

Using well-controlled external fields, we engineer spin interactions of the form

$$\begin{aligned} \hat{H}_B &= \sum_i \mathbf{B}_\mu \cdot \hat{\boldsymbol{\sigma}}_i \\ \hat{H}_I &= \frac{1}{N} \sum_{i < j} J_{i,j} \hat{\sigma}_i^z \hat{\sigma}_j^z \end{aligned} \quad (1)$$

where $\hat{\boldsymbol{\sigma}}_i = (\hat{\sigma}_i^x, \hat{\sigma}_i^y, \hat{\sigma}_i^z)$ is the vector of Pauli matrices for ion i . We label the qubit spin states $|\uparrow\rangle \equiv |m_s = +1/2\rangle$ and $|\downarrow\rangle \equiv |m_s = -1/2\rangle$, where m_s is the spin’s projection along the quantizing field $B_0 \hat{z}$, such that $\hat{\sigma}_i^z |\uparrow\rangle = |\uparrow\rangle$ and $\hat{\sigma}_i^z |\downarrow\rangle = -|\downarrow\rangle$. The Hamiltonian \hat{H}_B encodes an interaction due to an effective magnetic field, \mathbf{B}_μ (generated by externally applied microwaves at 124 GHz), that couples equally to all spins and permits global rotations (Fig. 1). The interaction \hat{H}_I describes a general coupling, $J_{i,j}$ between spins i and j a distance $d_{i,j}$ apart^{28,29}. For $J_{i,j} > 0$

¹US National Institute of Standards and Technology, Time and Frequency Division, Boulder, Colorado 80305, USA. ²Department of Physics, Georgetown University, Washington DC 20057, USA.

³Department of Physics, North Carolina State University, Raleigh, North Carolina 27695, USA. ⁴National Laser Centre, Council for Scientific and Industrial Research, Pretoria 0001, South Africa. ⁵Centre for Engineered Quantum Systems, School of Physics, The University of Sydney, New South Wales 2006, Australia.

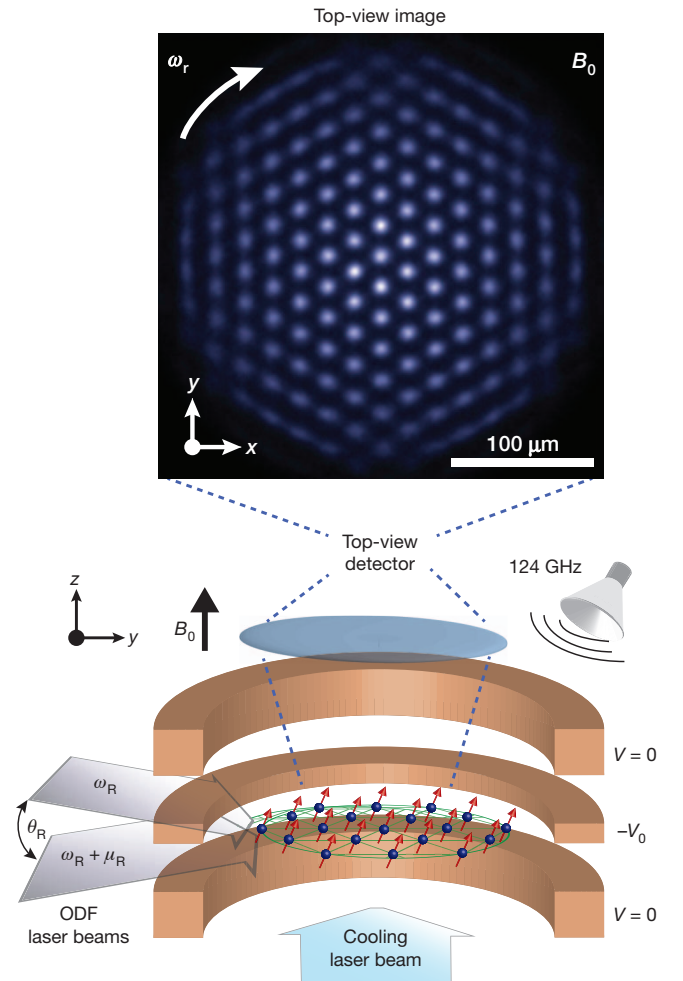


Figure 1 | The Penning trap confines hundreds of spin-1/2 qubits on a 2D triangular lattice. Each qubit is the valence-electron spin of a ${}^9\text{Be}^+$ ion. Bottom: a Penning trap confines ions using a combination of static electric and magnetic fields. The trap parameters are configured such that laser-cooled ions form a triangular 2D crystal. A general spin–spin interaction, \hat{H}_I , is generated by a spin-dependent excitation of the transverse (along z) motional modes of the ion crystal. This coupling is implemented using an optical dipole force (ODF) produced by a pair of off-resonance laser beams (left side) with angular separation θ_R and difference frequency μ_R . Microwaves at 124 GHz permit global spin rotations \hat{H}_B . Top: a representative top-view resonance fluorescence image showing the centre region of an ion crystal captured in the ions’ rest frame; in the laboratory frame, the ions rotate at $\omega_r = 2\pi \times 43.8$ kHz (ref. 26). Fluorescence is an indication of the qubit spin state ($|\uparrow\rangle$, bright; $|\downarrow\rangle$, dark); here, the ions are in the state $|\uparrow\rangle$. The lattice constant is $d_0 \approx 20$ μm .

the coupling is antiferromagnetic and for $J_{ij} < 0$ the coupling is ferromagnetic.

We implement \hat{H}_I using a spatially uniform, spin-dependent ODF generated by a pair of off-resonance laser beams with difference frequency μ_R (Fig. 1 and Supplementary Information). The ODF couples each ion’s spin to one or more of the N transverse (along z) motional modes of the Coulomb crystal by forcing coherent displacements of the ions that in turn modify the ions’ Coulomb potential energy through the interaction

$$\hat{H}_{\text{ODF}} = - \sum_i^N F_z(t) \hat{z}_i \hat{\sigma}_i^z$$

Here $F_z(t) = F_0 \cos(\mu_R t)$ is the ODF; $\hat{z}_i = \sum_{m=1}^N b_{i,m} \sqrt{\hbar/2M\omega_m}$ ($\hat{a}_m e^{-i\omega_m t} + \hat{a}_m^\dagger e^{i\omega_m t}$) is the axial position operator for ion i ; $b_{i,m}$ are elements of the N transverse phonon eigenfunctions, \mathbf{b}_m , at frequencies

ω_m , normalized as $\sum_{m=1}^N |b_{i,m}|^2 = \sum_{i=1}^N |b_{i,m}|^2 = 1$ (refs 28, 29); M is the ion mass; and \hbar is Planck’s constant divided by 2π . The modes include the centre-of-mass (COM) mode (ω_1) as well as an array of modes of higher spatial frequencies that may be derived from atomistic calculations (Fig. 2a) and confirmed by experimental measurement³⁰.

For small, coherent displacements, where residual spin–motion entanglement can be neglected²⁹ (Methods), \hat{H}_{ODF} is equivalent to \hat{H}_I in equation (1): spins i and j are coupled in proportion to their spin

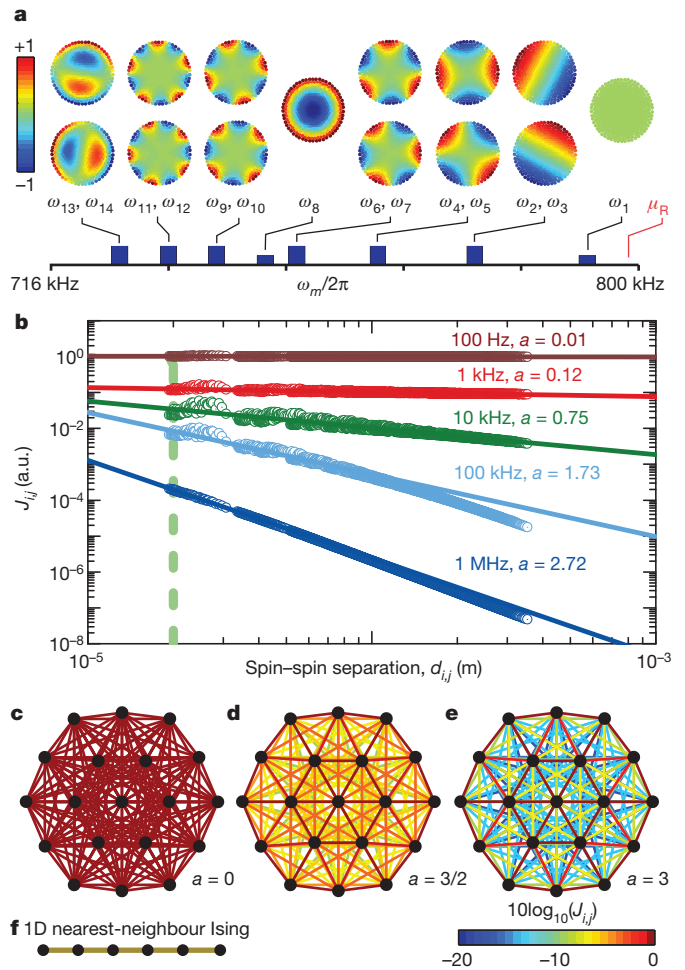


Figure 2 | Spin–spin interactions are mediated by the ion crystal’s transverse motional degrees of freedom. **a**, For a 2D crystal with $N = 217$ ions and $\omega_r = 2\pi \times 45.6$ kHz, we calculate the eigenfunctions, \mathbf{b}_m , and eigenfrequencies, ω_m , for the N transverse motional modes (Supplementary Information). Plotted here are ω_m and \mathbf{b}_m for the 14 highest-frequency modes. Relative mode amplitude is indicated by colour. The COM motion is the highest in frequency ($\omega_1 \approx 2\pi \times 795$ kHz); \mathbf{b}_1 has no spatial variation. The lowest-frequency mode is $\omega_{217} \approx 2\pi \times 200$ kHz; \mathbf{b}_{217} has spatial variation at the lattice-spacing length scale, $d_0 \approx 20$ μm . **b**, Using equation (2), we calculate J_{ij} explicitly for $N = 217$ spins and plot it as a function of spin–spin separation, d_{ij} . For $\mu_R - \omega_1 < 2\pi \times 1$ kHz, \hat{H}_{ODF} principally excites COM motion in which all ions equally participate: the spin–spin interaction is spatially uniform. As the detuning is increased, modes of higher spatial frequency participate in the interaction and J_{ij} develops a finite interaction length. We find the scaling of J_{ij} with d_{ij} follows the power law $J_{ij} \propto d_{ij}^{-a}$. For $\mu_R - \omega_1 \gg 2\pi \times 500$ kHz, all transverse modes participate and the spin–spin coupling power-law exponent, a , approaches 3. The solid lines are power-law fits to the theory points. For comparison with other experiments, the nearest-neighbour coupling ($d_0 = 20$ μm) is marked by the dashed line. **c–e**, The power-law nature of J_{ij} is qualitatively illustrated for $N = 19$ (for larger N , diagrams of similar size are illegible). Spins (nodes) are joined by lines coloured in proportion to their coupling strength for various values of a . **f**, For context, the graph for a 1D nearest-neighbour Ising interaction, a well-known model in quantum field theory, is plotted.

states, $\hat{\sigma}_i^z$ and $\hat{\sigma}_j^z$, and by their mutual participation in each motional mode m . The coupling coefficient is given by²⁹

$$J_{ij} = \frac{F_0^2 N}{2\hbar M} \sum_{m=1}^N \frac{b_{i,m} b_{j,m}}{\mu_R - \omega_m^2} \quad (2)$$

These pairwise interaction coefficients can be calculated explicitly by use of the ion motional modes. We find that the range of interaction can be modified by detuning away from the COM mode as shown in Fig. 2b. In the limit $\mu_R - \omega_1 \gg 2\pi \times 500$ kHz, all modes participate equally in the interaction and $J_{ij} \propto d_{ij}^{-3}$, as discussed in ref. 28. At intermediate detuning, we find a power-law scaling of the interaction range, $J_{ij} \propto d_{ij}^{-a}$, where a can be tuned within the range $0 \leq a \leq 3$. That is, by adjusting the single experimental parameter, μ_R , we can mimic a continuum of physical couplings including important special cases: infinite range ($a = 0$); monopole–monopole, or Coulomb-like ($a = 1$); monopole–dipole ($a = 2$); and dipole–dipole ($a = 3$). The choice of $a = 0$ results in the ‘ \hat{J}_z^2 interaction’, which gives rise to spin squeezing and is used in quantum logic gates²⁷ (Supplementary Information). In addition, tuning μ_R also gives access to both antiferromagnetic ($\mu_R > \omega_1$) and ferromagnetic ($\omega_2 \ll \mu_R < \omega_1$) couplings^{10,13}.

Experimentally, we demonstrate a tunable-range Ising interaction by observing a global spin precession under the application of \hat{H}_I (Fig. 3). We compare experimental data with the mean-field prediction that the influence of \hat{H}_I on spin j can be modelled as a magnetic field $\bar{B}_j = (2/N) \sum_{i,i \neq j} J_{ij} \langle \hat{\sigma}_i^z \rangle$ in the z direction due to the remaining $N - 1$ spins (Supplementary Information; angle brackets denote expectation value). For a general qubit superposition state, \bar{B}_j gives rise to spin precession about z in excess of that expected to result from simple Larmor precession (Fig. 3b). The experiment sequence shown in Fig. 3a measures this excess precession, averaged over all spins in the crystal. At the outset, each spin is prepared in state $|\uparrow\rangle$ and then rotated about the x axis by angle θ_1 . The interaction \hat{H}_I is applied during the arms of a spin echo, each of duration τ_{arm} ; precession proportional to $\langle \hat{\sigma}_i^z \rangle$ coherently adds throughout the interaction duration, $2\tau_{\text{arm}}$. The final $\pi/2$ -pulse maps precession out of the initial plane (y - z) into excursions along z (above or below the equatorial plane of the Bloch sphere) that are resolved by projective spin measurement along z .

We detect global, state-dependent fluorescence ($|\uparrow\rangle$, bright; $|\downarrow\rangle$, dark) as a function of θ_1 using a photomultiplier tube. This measurement permits a systematic study of the mean-field-induced spin precession averaged over all particles

$$\frac{1}{N} \sum_j \bar{B}_j = 2 \left(\frac{1}{N^2} \sum_j \sum_{i,i \neq j} J_{ij} \right) \cos(\theta_1) \equiv 2\bar{J} \cos(\theta_1)$$

The probability of detecting state $|\uparrow\rangle$ at the end of the sequence is

$$P(|\uparrow\rangle) = \frac{1}{2} (1 + \exp(-\Gamma \cdot 2\tau_{\text{arm}}) \sin(\theta_1) \sin(2\bar{J} \cos(\theta_1) \cdot 2\tau_{\text{arm}})) \quad (3)$$

and a single-parameter fit to experimental data yields \bar{J} . Decoherence due to spontaneous emission is accounted for by Γ and is determined by independent measurement of the ODF laser beam intensities, I_R ($\Gamma \propto I_R$; see Supplementary Information).

In Fig. 3c, d, we show representative measurements of excess precession due to \hat{H}_I for different values of spin coupling strength (determined by $J_{ij} \propto I_R^2$) and interaction duration ($2\tau_{\text{arm}}$). The excess spin precession varies periodically with θ_1 (with period π) and greater interaction strengths result in more precession, manifested in our experiment as a larger amplitude modulation of $P(|\uparrow\rangle)$. Our data agree with equation (3) and allow direct extraction of \bar{J} for given experimental conditions. In Fig. 3e, we plot \bar{J} , normalized by I_R^2 (I_R is independently measured), as a function of the detuning $\mu_R - \omega_1$ ($N = 206 \pm 10$ ions). Using no free parameters, we find excellent agreement with the value of \bar{J} obtained by averaging over all J_{ij} , where the J_{ij} were calculated by including couplings to all N transverse modes (equation (2)).

The mean-field interpretation of our benchmarking measurement applies only for weak spin–spin correlations. Therefore, in the benchmarking regime we apply a weak interaction ($\bar{J} \cdot 2\tau_{\text{arm}} \ll \sqrt{N}/4$; see

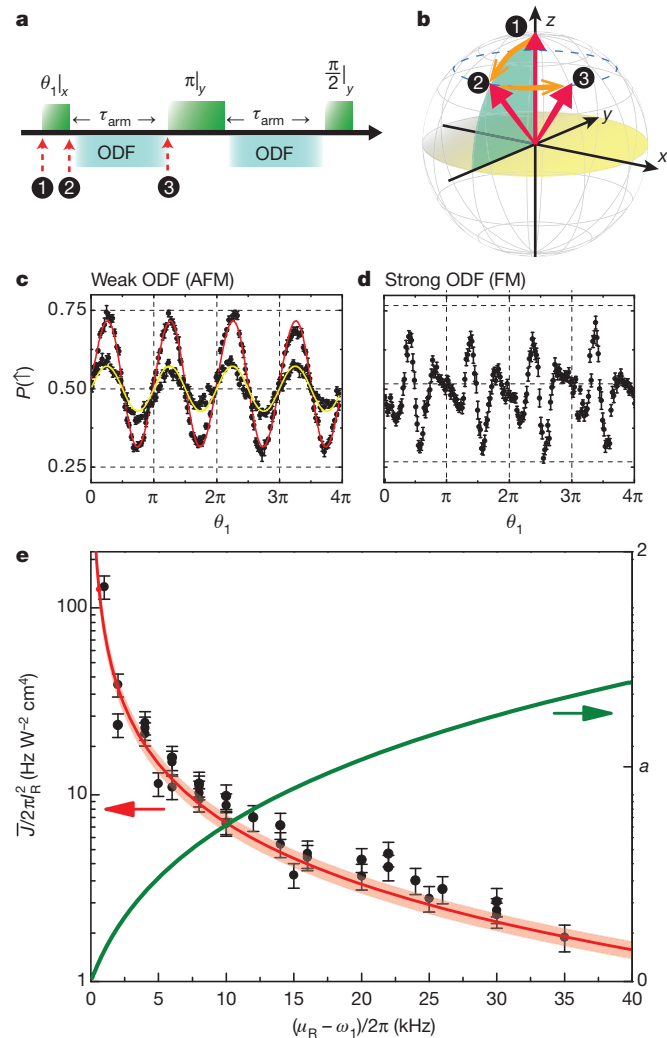


Figure 3 | Benchmarking the 2D Ising interaction. **a**, Spin-precession benchmarking sequence for \hat{H}_I . The spins are prepared at the outset in $|\uparrow\rangle$ (a ferromagnetic state). The spin–spin interaction, \hat{H}_I , is present when the ODF laser beams are on. We choose $\mu_R - \omega_1 = n \cdot 2\pi/\tau_{\text{arm}}$ so that for small detunings from the COM mode (ω_1), the spins are decoupled from the motion by the end of each period τ_{arm} . **b**, Evolution of a single spin before the application of the spin echo π -pulse. **c**, **d**, Plots showing spin precession proportional to $\langle \hat{\sigma}_z \rangle$ as a function of initial ‘tipping angle’ θ_1 . The error bars are statistical (s.d., 200 measurements). The plots show typical experimental data (black) and, in **c**, single-parameter fits to equation (3). For an antiferromagnetic (AFM) coupling, $\tau_{\text{arm}} = 250 \mu\text{s}$, $\mu_R - \omega_1 = 2\pi \times 4.0$ kHz and $I_R = 1.4 \text{ W cm}^{-2}$, we obtain $\bar{J}/I_R^2 = 2\pi \times 25 \text{ Hz W}^{-2} \text{ cm}^4$ (yellow fit). Longer drive periods and higher laser intensity, I_R , yield a larger precession. For $\tau_{\text{arm}} = 350 \mu\text{s}$, $\mu_R - \omega_1 = 2\pi \times 2.9$ kHz and $I_R = 1.9 \text{ W cm}^{-2}$, we obtain $\bar{J}/I_R^2 = 2\pi \times 55 \text{ Hz W}^{-2} \text{ cm}^4$ (red fit). The data in this plot is typical of the experiments conducted for benchmarking. For a much stronger interaction (**d**), equation (3) cannot be used to obtain \bar{J} because the mean-field assumption is no longer valid (Supplementary Information). Also, here we used a small negative detuning ($\omega_2 \ll \mu_R < \omega_1$), which gives a long-range ferromagnetic (FM) interaction. For these experiments, we set $\omega_r = 2\pi \times 45.6$ kHz. **e**, Benchmarking results for an ion crystal with $N = 206 \pm 10$ ions. Each point is generated by measuring \bar{J} as in **c**) and measuring the laser beam intensity, I_R , at the ions. The error bars are dominated by uncertainty in I_R (Supplementary Information). The solid line (red) is the prediction of mean-field theory that accounts for couplings to all N transverse modes; there are no free parameters. The line’s breadth reflects experimental uncertainty in the angle $\theta_R = 4.8 \pm 0.25^\circ$. The mean-field prediction for the average value of the power-law exponent, a , is drawn in green (right axis, linear scale).

Supplementary Information). In a quantum simulation, the same interaction is applied at greater power, producing quantum spin–spin correlations. In the present configuration of our apparatus, spontaneous emission due to the ODF laser beams (parameterized by Γ in equation (3)) is the dominant source of decoherence. With modest laser powers of 4 mW per laser beam and a detuning of $\mu_R - \omega_1 = 2\pi \times 2$ kHz, we obtain $\bar{J} \approx 2\pi \times 0.5$ kHz and $\Gamma/\bar{J} \approx 0.06$. The expected spin squeezing (\bar{J}_z^2) due to this interaction is 5 dB (limited by spontaneous emission). The ratio Γ/\bar{J} can be reduced by a factor of 50 by increasing the ODF laser beams' angular separation, θ_R , to 35° (Fig. 1), which is a likely prerequisite for access to the shortest-range, dipole–dipole, coupling regime ($a \rightarrow 3$). At present, geometric constraints impose the limit $\theta_R < 5^\circ$; we plan upgrades to our apparatus to permit $\theta_R = 35^\circ$. Thus far we operated with ODF magnitudes equal but opposite for $|\uparrow\rangle$ and $|\downarrow\rangle$; relaxation of this constraint can further reduce Γ/\bar{J} .

Our work establishes the suitability of Penning traps for simulation of quantum magnetism in a regime inaccessible to classical computation. Our approach is based on naturally occurring 2D Coulomb (Wigner) crystals with hundreds of ion qubits, a novel experimental system that does not require demanding trap-engineering efforts. Experimentally, we used an ODF to engineer a tunable-range spin–spin interaction and benchmarked the interaction strength. Excellent agreement was obtained with the predictions of mean-field theory and atomistic calculations that predict a power-law antiferromagnetic spin coupling, $J_{ij} \propto d_{ij}^{-a}$, for $0.05 \lesssim a \lesssim 1.4$.

With this work as a foundation, we anticipate a variety of future investigations. For example, simultaneous application of the non-commuting interactions \hat{H}_B and \hat{H}_I is expected to give rise to quantum phase transitions; \hat{H}_I may be antiferromagnetic ($\mu_R > \omega_1$) or ferromagnetic ($\omega_2 \ll \mu_R < \omega_1$). Geometric modifications to our apparatus will permit access to larger values of θ_R and antiferromagnetic dipole–dipole-type couplings ($a \rightarrow 3$). Improved image processing software will permit direct measurement of spin–spin correlation functions using our existing single-spin-resolving imaging system (Fig. 1).

METHODS SUMMARY

In a frame rotating at frequency ω , the trap potential is

$$q\phi(r, z) = \frac{1}{2}M\omega_1^2(z^2 + \beta r^2)$$

where $\beta = \omega_r \omega_1^{-2}(\Omega_c - \omega_1) - 1/2$. The $^9\text{Be}^+$ cyclotron frequency is $\Omega_c = B_0 q/M = 2\pi \times 7.6$ MHz and the frequency of the ions' harmonic COM motion along z is $\omega_1 = 2\pi \times 795$ kHz. Ion rotation is precisely controlled with an external rotating quadrupole potential²⁶. For $100 \lesssim N \lesssim 350$, we set $\omega_r \approx 2\pi \times 45$ kHz so that the radial confinement is weak enough that a cloud of ions relaxes into a single 2D plane ($\beta \ll 1$). When the ions' motional degrees of freedom are Doppler laser cooled³⁰ ($T_{\text{COM}} \approx 1$ mK), the ions naturally form a 2D Coulomb crystal on a triangular lattice, which is the geometry that minimizes the energy of their mutual Coulomb potential energy. The crystal has N transverse eigenmodes, ω_m , with eigenfunctions \mathbf{b}_m ; the COM mode, ω_1 , is the highest-frequency mode (Fig. 2a).

The spin-dependent ODF is generated by a pair of off-resonance laser beams with angular separation $\theta_R \approx 4.8^\circ$ and difference frequency μ_R (Fig. 1). The result is a travelling 1D optical lattice of wavelength $\lambda_R = 2\pi/\Delta k \approx 3.7$ μm whose wavefronts propagate along z , traversing the ion crystal at frequency $\mu_R/2\pi$. Alignment of the optical lattice is crucial for proper spin–spin coupling (Supplementary Information). The lattice's polarization gradient induces a differential a.c. Stark shift on the qubit states (a spin-dependent force). We choose operating conditions that give $\mathbf{F}_\uparrow \approx -\mathbf{F}_\downarrow$, where $\mathbf{F}_\uparrow = F_0 \cos(\mu_R t)\hat{\mathbf{z}}$. For reference, if the single-beam intensity at the ions is $I_R = 1$ W cm^{-2} , we obtain $F_0 \approx 1.4 \times 10^{-23}$ N.

Small, coherent displacements that produce negligible spin–motion entanglement (as required by equation (2)) are obtained for detunings satisfying

$$\hbar|\mu_R - \omega_m| > F_0 \sqrt{\hbar(2\bar{n}_m + 1)/2M\omega_m}$$

This is a more stringent criterion than that used by others^{13,29}, because it includes an additional factor of \sqrt{N} to account for a typical distribution of composite spin states. Moreover, we also include a correction factor for finite temperature, $\bar{n}_m \approx k_B T/\hbar\omega_m$, where k_B is the Boltzmann constant.

Received 16 November 2011; accepted 21 February 2012.

- Anderson, P. W. The resonating valence bond state in La_2CuO_4 and superconductivity. *Science* **235**, 1196–1198 (1987).
- Moessner, R., Sondhi, S. L. & Chandra, P. Two-dimensional periodic frustrated Ising models in a transverse field. *Phys. Rev. Lett.* **84**, 4457–4460 (2000).
- Sandvik, A. W. Ground states of a frustrated quantum spin chain with long-range interactions. *Phys. Rev. Lett.* **104**, 137204 (2010).
- Feynman, R. Simulating physics with computers. *Int. J. Theor. Phys.* **21**, 467–488 (1982).
- Buluta, I. & Nori, F. Quantum simulators. *Science* **326**, 108–111 (2009).
- Trotzky, S. *et al.* Time-resolved observation and control of superexchange interactions with ultracold atoms in optical lattices. *Science* **319**, 295–299 (2008).
- Lin, Y.-J., Compton, R. L., Jiménez-García, K., Porto, J. V. & Spielman, I. B. Synthetic magnetic fields for ultracold neutral atoms. *Nature* **462**, 628–632 (2009).
- Jo, G.-B. *et al.* Itinerant ferromagnetism in a Fermi gas of ultracold atoms. *Science* **325**, 1521–1524 (2009).
- Friedenaauer, A., Schmitz, H., Glueckert, J. T., Porras, D. & Schaetz, T. Simulating a quantum magnet with trapped ions. *Nature Phys.* **4**, 757–761 (2008).
- Kim, K. *et al.* Quantum simulation of frustrated Ising spins with trapped ions. *Nature* **465**, 590–593 (2010).
- Simon, J. *et al.* Quantum simulation of antiferromagnetic spin chains in an optical lattice. *Nature* **472**, 307–312 (2011).
- Ma, X.-s., Dakic, B., Naylor, W., Zeilinger, A. & Walther, P. Quantum simulation of the wavefunction to probe frustrated Heisenberg spin systems. *Nature Phys.* **7**, 399–405 (2011).
- Islam, R. *et al.* Onset of a quantum phase transition with a trapped ion quantum simulator. *Nature Commun.* **2**, 377 (2011).
- Lanyon, B. P. *et al.* Universal digital quantum simulation with trapped ions. *Science* **334**, 57–61 (2011).
- Sachdev, S. *Quantum Phase Transitions* (Cambridge Univ. Press, 2001).
- Kohn, M., Starykh, O. a. & Balents, L. Spins and triplons in spatially anisotropic frustrated antiferromagnets. *Nature Phys.* **3**, 790–795 (2007).
- Varney, C., Sun, K., Galitski, V. & Rigol, M. Kaleidoscope of exotic quantum phases in a frustrated XY model. *Phys. Rev. Lett.* **107**, 077201 (2011).
- Levi, B. G. New candidate emerges for a quantum spin liquid. *Phys. Today* **60**, 16–19 (2007).
- Helton, J. S. *et al.* Spin dynamics of the spin-1/2 Kagome lattice antiferromagnet $\text{ZnCu}_3(\text{OH})_6\text{Cl}_2$. *Phys. Rev. Lett.* **98**, 107204 (2007).
- Balents, L. Spin liquids in frustrated magnets. *Nature* **464**, 199–208 (2010).
- Lewenstein, M. *et al.* Ultracold atomic gases in optical lattices: mimicking condensed matter physics and beyond. *Adv. Phys.* **56**, 243–379 (2007).
- Bloch, I. & Zewiger, W. Many-body physics with ultracold gases. *Rev. Mod. Phys.* **80**, 885–964 (2008).
- Rosenband, T. *et al.* Frequency ratio of Al^+ and Hg^+ single-ion optical clocks; metrology at the 17th decimal place. *Science* **319**, 1808–1812 (2008).
- Schmied, R., Wesenberg, J. H. & Leibfried, D. Optimal surface-electrode trap lattices for quantum simulation with trapped ions. *Phys. Rev. Lett.* **102**, 233002 (2009).
- Biercuk, M. J. *et al.* High-fidelity quantum control using ion crystals in a Penning trap. *Quantum Inf. Comput.* **9**, 920–949 (2009).
- Mitchell, T. *et al.* Direct observations of structural phase transitions in planar crystallized ion plasmas. *Science* **282**, 1290–1293 (1998).
- Leibfried, D. *et al.* Experimental demonstration of a robust, high-fidelity geometric two ion-qubit phase gate. *Nature* **422**, 412–415 (2003).
- Porras, D. & Cirac, J. Quantum manipulation of trapped ions in two dimensional coulomb crystals. *Phys. Rev. Lett.* **96**, 250501 (2006).
- Kim, K. *et al.* Entanglement and tunable spin–spin couplings between trapped ions using multiple transverse modes. *Phys. Rev. Lett.* **103**, 120502 (2009).
- Sawyer, B. C. *et al.* Spectroscopy and thermometry of drumhead modes in a mesoscopic trapped-ion crystal using entanglement. *Phys. Rev. Lett.* (in the press); preprint at (<http://arxiv.org/abs/1201.4415>) (2012).

Supplementary Information is linked to the online version of the paper at www.nature.com/nature.

Acknowledgements This work was supported by the DARPA OLE programme and NIST. A.C.K. was supported by the NSF under grant number DMR-1004268. B.C.S. is supported by an NRC fellowship funded by NIST. J.K.F. was supported by the McDevitt endowment bequest at Georgetown University. M.J.B. and J.J.B. acknowledge partial support from the Australian Research Council Center of Excellence for Engineered Quantum Systems CE110001013. We thank F. da Silva, R. Jordens, D. Leibfried, A. O'Brien, R. Scalettar and A. M. Rey for discussions.

Author Contributions J.W.B., B.C.S., H.U., M.J.B. and J.J.B. designed the experiment. J.W.B. and B.C.S. obtained the data and analysed it with advice from J.J.B., A.C.K., C.-C.J.W. and J.K.F. developed the formalism and numerics to calculate the spin–spin coupling. J.W.B. wrote the manuscript with assistance from B.C.S., M.J.B. and J.J.B. All authors participated in discussions, contributed ideas throughout the project and edited the manuscript.

Author Information This manuscript is a contribution of the US National Institute of Standards and Technology and is not subject to US copyright. Reprints and permissions information is available at www.nature.com/reprints. The authors declare no competing financial interests. Readers are welcome to comment on the online version of this article at www.nature.com/nature. Correspondence and requests for materials should be addressed to J.W.B. (joe.britton@gmail.com).